Optical properties of phosphorus-related point defects in silica fiber preforms

Giusy Origlio
Laboratoire H. Curien, UMR CNRS 5516, Université Jean Monnet, 18 rue du Pr. Benoît Lauras, 42000 Saint-Etienne, France and Dipartimento di Scienze Fisiche ed Astronomiche, dell'Università di Palermo, I-90123 Palermo, Italy

Fabrizio Messina,* Marco Cannas, and Roberto Boscaino
Dipartimento di Scienze Fisiche ed Astronomiche, dell'Università di Palermo, I-90123 Palermo, Italy

Sylvain Girard
CEA, DAM, DIF, F91297 Arpajon, France

Aziz Boukenter and Youcef Ouerdane
Laboratoire H. Curien, UMR CNRS 5516, Université Jean Monnet, 18 rue du Pr. Benoît Lauras, 42000 Saint-Etienne, France
(Received 9 September 2009; revised manuscript received 15 October 2009; published 30 November 2009)

We report an experimental study on phosphorus-related point defects in amorphous silica, based on photoluminescence, absorption, and electron spin resonance measurements carried out on P-doped SiO_2 fiber preforms. By photoluminescence measurements excited by laser or synchrotron light we detect an emission band peaked at 3.0 eV with a lifetime in the range of ms. The excitation spectrum of the 3.0 eV emission consists of two transitions peaked at 4.8 and 6.4 eV, the former giving rise also to a measurable absorption band. We attribute this optical activity to a P-related point defect embedded in SiO_2, based on the spatial correlation between the emission intensity and the P doping level. A detailed spectroscopical investigation allows us to propose a scheme of the electronic levels of this P-related defect, in which the 4.8 and 6.4 eV excitation channels arise from transitions from the ground to two-excited singlet states, while the long-lived 3.0 eV emission is associated to a spin-forbidden transition from an excited triplet to the ground state. Finally, electron spin resonance measurements on *X*-irradiated samples lead us to propose a tentative microscopic model of the defect as a diamagnetic four-coordinated P impurity substitutional to a Si atom.

DOI: 10.1103/PhysRevB.80.205208 PACS number(s): 71.55.Jv, 78.47.Cd, 82.50.Kx

I. INTRODUCTION

Phosphorus-doped silica is a material of fundamental importance in optical communications and in microelectronics. P doping is often used in optical fibers to achieve an optimal refractive index profile[1] and to modify the viscosity of the core and cladding regions.[2] Phosphate glasses are potentially good ultraviolet (UV) transmitting materials allowing the fabrication of thin glass films for application in microlithography and laser systems.[2] P-doping allows to greatly increase the efficiency of rare-earth based optical amplifiers[3] and phosphosilicate glass are promising candidates as radiation sensors due to their closely linear response to radiation dose.[4] Finally, it has been reported that strong photosensitive properties can be induced in P-doped silica by hydrogen loading or high temperature treatment in a hydrogen-oxygen flame.[5,6] A thorough understanding of the microscopic arrangements of P impurities in silica, as well as of the properties of the resulting P-related point defects, would be potentially useful to optimize the performance of P-doped SiO_2 in applications.

Most of the current understanding of P-related defects in SiO_2 derives from electron spin resonance (ESR) experiments on irradiated phosphosilicate glasses. ESR allowed to identify unambiguously four main P-related paramagnetic point defects, referred to as P4, P1, P2, and POHC centers.[7–9] In P4, P1, and P2, the unpaired electron is localized on the central P atom, bonded to a different number of oxygen atoms, 2, 3, and 4, respectively.[6,8,10–12] Hence, their structure can be represented as $[(O\text{-})_2P^{\bullet}]^0$, $[(O\text{-})_3P^{\bullet}]^+$ and $[(O\text{-})_2P^{\bullet}(\text{-}O)_2]^0$, respectively, where • represents an unpaired electron.[20] The paramagnetic signal of POHC is ubiquitous in P_2O_5-containing glasses. In the simplest model of this defect, the P atom is bonded to three bridging O atoms and to a fourth nonbridging O which hosts the unpaired electron: $[(O\text{-})_3P\text{-}O^{\bullet}]^+$. However, this structure (here referred to as l-POHC) has been argued to be stable only at low temperature, while the room-temperature stable form of POHC (here referred to as r-POHC) was proposed to feature an electron shared by two nonbridging oxygen atoms bonded to the same phosphorus $[(O\text{-})_2P(\text{-}O)_2^{\bullet}]^0$.[8] l-POHC and r-POHC supposedly feature two slightly different ESR signals. After clarifying by ESR the microscopic structure of these defects, data obtained by optical absorption (OA) studies of irradiated P-doped silica were interpreted by proposing associations between some of the observed OA bands and the paramagnetic centers.[6,8]

In contrast, much less is known about diamagnetic P-related centers in SiO_2. Based on the results obtained by several independent experimental techniques, including Raman and infrared measurements, phosphosilicate glass is generally believed to consist of an intermixed random network of $[(O\text{-})_2Si(\text{-}O)_2]^0$ and $[(O\text{-})_3P{=}O]^0$ tetrahedra randomly bonded by sharing O atoms, this being consistent with the fact that $[(O\text{-})_3P{=}O]^0$ is the basic building block of pure stoichiometric (P_2O_5) phosphate glass.[13–16] In this model each P atom is bonded to three bridging O atoms and a single doubly-bond nonbridging O, and thus each site can be argued

to be a potential precursor for l-POHC via ionization of the nonbridging oxygen. In contrast, r-POHC should be formed by ionization of a defective site $[(O\text{-})_2P(=O)_2]^-$ where the P atom bonds two bridging oxygen atoms with single bonds and two more nonbridging oxygen with double bonds.[8] Finally, P4, P1, and P2 centers are supposedly formed by irradiation via hole or electron trapping on hypothetical diamagnetic precursor defects where P is two-, three-, and four-fold coordinated, respectively:[21] $[(O\text{-})_2P:]^-$, $[(O\text{-})_3P:]^0$, and $[(O\text{-})_2P(\text{-}O)_2]^+$.[6,8,10,11] In the intermixed random network model, also these sites should be considered as randomly occurring point defects.

From the experimental point of view, the optical properties of diamagnetic P-related centers in silica are scarcely known at the moment, since only very little data exist on optical absorption and luminescence of as-grown phosphosilicate glasses, expect for the basic evidence that no strong UV absorption bands are generally induced in these materials just by P-doping.[6,17] The purpose of this work is to contribute to a better understanding of these topics, by reporting data obtained by absorption and photoluminescence measurements in the UV and vacuum UV spectral ranges on P-doped optical fiber preforms.

II. EXPERIMENTAL METHODS

The experimental data reported in this paper were obtained on multistep-index P-doped fiber preforms provided by iXFiber S.A.S. The samples are made up of an outer undoped high purity silica layer and four internal cylindrical layers (core part, zones 1–4) of highly pure synthetic silica doped with different P amounts. Phosphorus doping profile grows from the boundaries to the center following a multiple step distribution as shown in the microscopic image of Fig. 1.

The layers were deposited inside a tube of undoped fused silica, which forms the cladding (zone 0). The core-cladding part is made with modified chemical vapor deposition (MCVD) process and does not contain a relevant concentration of extrinsic impurities, except for chlorine that is present with a maximum concentration of ~0.2 wt. %. The preforms had an initial diameter of 12.84 mm with a 5 mm doped region and they were subsequently cut into $6\times6\times1.5$ mm^3 samples and polished. Phosphorus and chlorine concentrations were checked by electron microprobe analysis, giving the results shown in Fig. 1. The preform characteristics are summarized in Table I.

Photoluminescence (PL) time-resolved measurements excited in the UV range were performed using a pulsed laser system (VIBRANT OPOTEK) with a pulse width of 5 ns, a repetition rate of 10 Hz and an energy density per pulse of (0.27 ± 0.02) mJ/cm^2. The emitted light was dispersed by a spectrograph equipped with a 150 grooves/mm grating, blazed at 300 nm with a spectral bandwidth of 3 nm, and then acquired by an intensified charge coupled device (CCD) camera. The acquisition is gated within a time window of width W_T, which opens starting from a delay time T_D with respect to the laser pulse. All the spectra were corrected for the spectral response and the spectrograph dispersion.

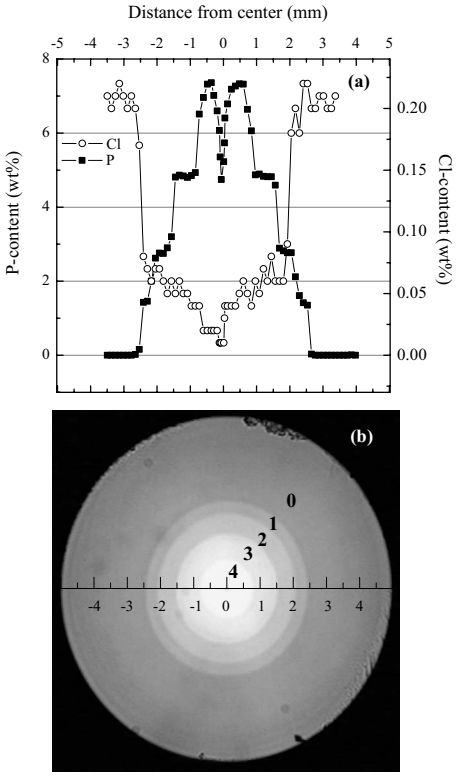

FIG. 1. (a): P content (full squares) and Cl content (empty circles) obtained by electron microprobe analysis at various distances from the preform center. (b): Enlarged view of the sample. Numbers from 0 to 4 refer to the various sample zones listed in Table I with different P amounts. The *x* scales in the upper and lower figures coincide.

Excitation (PLE) and emission spectra excited in the vacuum UV (VUV) range, were carried out under excitation by pulsed synchrotron radiation in the range 4.5–9.0 eV, with a pulse width of 130 ps, an interpulse of 500 ns, and a spectral width of 0.3 nm, at the SUPERLUMI station on the I-beamline of HASYLAB at DESY (Hamburg). The emitted light was spectrally dispersed by a 300 grooves/mm grating blazed at 300 nm and acquired by a liquid nitrogen cooled CCD camera (1100 Princeton instruments) for PL spectra or by a photomultiplier (Hamamatsu R2059) for PLE spectra. PL spectra were corrected both for the spectral response and dispersion of the detecting system, while excitation spectra were corrected for the spectral efficiency of the exciting light. Excitation bandwidth was 0.3 nm, while emission bandwidth was 20 nm.

OA spectra on preform samples were carried out by the Jasco V-560 spectrophotometer in the 3.5–6.0 eV spectral range. VUV absorption spectra in the 6.0–7.5 eV range were obtained using an ACTON SP-150 single-beam spectrophotometer, equipped with a 30 W D_2 lamp and two 1200 lines/mm monochromators and working in N_2 flux. The acquired spectra were corrected by subtracting the contribution due to surface reflectance.

During laser-excited luminescence and optical absorption measurements, we put the sample behind a properly built mask so as to be sure that laser light excited only the central region (zone 4) of the preform. On the contrary, synchrotron

TABLE I. Parameters related to P-doped preform samples. Δn refers to the refractive index change at $\lambda = 633$ nm with respect to silica.

	Zone	⟨P⟩ (wt. %)	⟨Cl⟩ (wt. %)	Δn ($\times 10^{-3}$)	Preform diam. (mm)	Fiber diam. (μm)
Cladding	0	0.00	0.23	0.46	12.8	125.0
Core	1	1.63	0.07	1.37	5.0	62.5
	2	3.17	0.06	2.58	4.2	52.8
	3	5.05	0.05	4.80	3.1	38.8
	4	7.09	0.02	7.08	1.6	19.4

excitation did not allow to spatially resolve the different sample zones. In both the experimental setups, temperature dependencies (from 10 to 300 K) were investigated using continuous flow helium cryostats. Finally, ESR measurements were carried out at room temperature by a Bruker EMX spectrometer working at 9.7 GHz (*X* band) on the pristine preform and on samples irradiated by 10 keV x-rays at room temperature using the ARACOR facility at the French atomic energy center (CEA).

III. RESULTS

Figure 2 shows the OA spectrum of the central zone of the sample (zone 4, maximum P content $\simeq 7$ wt. %) in the UV and in the VUV spectral range.

It is evident the presence of a strong absorption band in the VUV range centered at about 6.9 eV, an absorption tail for $E > 7$eV, and a shoulder in the UV region, due to a band centered at about 4.8 eV (inset of Fig. 2).

By performing a PL emission measurement at room temperature under synchrotron excitation at the energy corresponding to the UV band (4.8 eV), we detected a broad asymmetric luminescence signal centered at 3.0 eV, reported in Fig. 3(a). The PLE spectrum of this signal, measured with emission at $E_{em} = 3$ eV, is reported in Fig. 3(b) and features two components: the first one is centered at 4.7 eV (with FWHM ~ 0.7 eV) and the second one at 6.4 eV (with FWHM ~ 0.6 eV). The shape of the emission band turns out to be approximately the same when excited at 4.8 eV (full squares) or 6.4 eV (open circles) by synchrotron radiation, or upon laser excitation at 4.8 eV (solid line), as shown by the comparison of the three signals in Fig. 3(a).

We studied the dependence of the 3.0 eV luminescence signal intensity on P concentration, by moving the laser excitation spot across the different preform zones via a micropositioning stage. The spatial resolution of this measurement is limited by the diameter of the laser spot, partialized by an iris that is about 0.5 mm. As shown in Fig. 4(a), we found that the 3.0 eV PL signal is observed only in the P-doped region of the sample and rapidly disappears when moving away from the center of the perform. By comparing with the spatial dependence of P concentration, we see that the luminescent region is somewhat narrower than the doped region. Indeed, the 3.0 eV PL is mainly localized on zones III and IV of the preform. Figure 4(b) shows the PL intensity on the peak of the 3.0 eV band as a function of P content. It appears that the luminescence signal shows up only when P concentration overcomes a $\sim 4\%$ threshold.

We performed time-resolved emission measurements (Fig. 5) on the 3.0 eV band, by acquiring at room temperature several emission spectra upon laser excitation, with $W_T = 500$ μs and T_D going from 1 μs to 25 ms. These data allow to study the decay kinetics of the PL signal at several spectral positions within the emission band. Since the decay turns out to be single exponential at any fixed emission en-

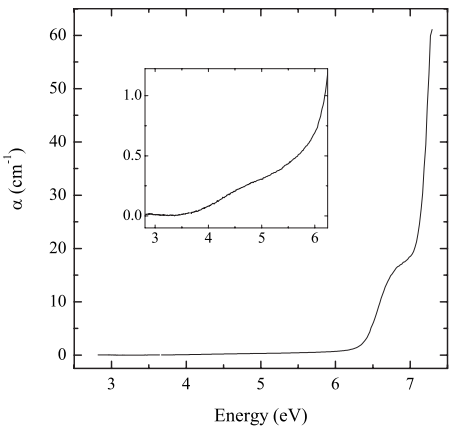

FIG. 2. Absorption spectrum of the P-doped preform in the UV-VUV spectral range (2.5–7.5 eV). The inset shows the enlargement of the OA spectrum from 3 to 6 eV.

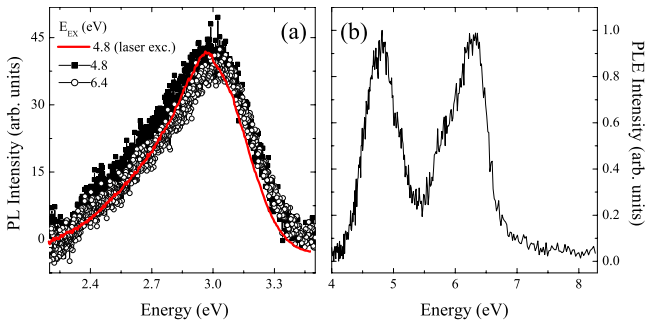

FIG. 3. (Color online) (a): Emission spectra measured in the central sample zone (zone 4), containing ~ 7 wt. % of phosphorus at 300 K, obtained exciting at 4.8 eV (full squares) and 6.4 eV (open circles) under synchrotron radiation and at 4.8 eV under laser excitation with $W_T = 20$ ms and $T_D = 5$ ns (solid line). (b): Excitation spectrum monitored at $E_{em} = 3$ eV detected at room temperature under synchrotron radiation in the range 4–8.3 eV.

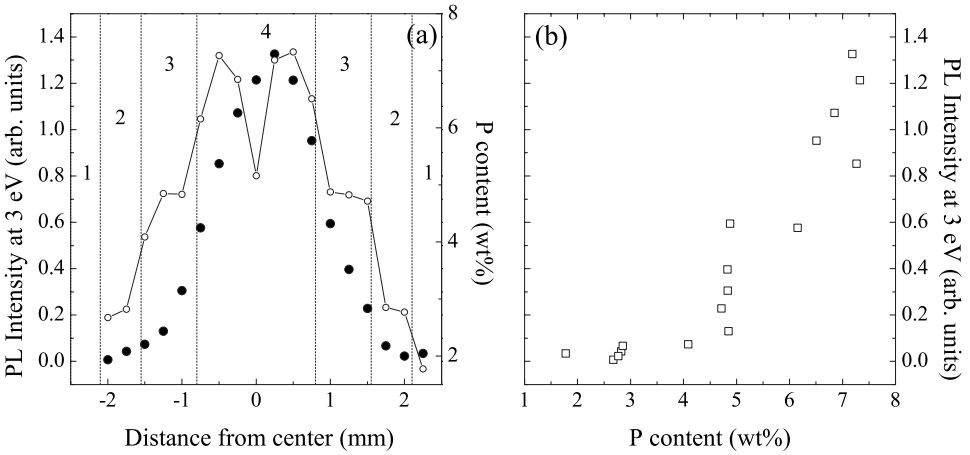

FIG. 4. (a): PL intensity at 3 eV measured at room temperature under laser excitation at 4.8 eV with W_T=20 ms and T_D=5 ns (full circles, left vertical scale) and phosphorus content (open circles, right vertical scale) as a function of the distance from the preform center. Vertical lines refer to the different sample zones (from 1 to 4) as listed in Table I and in Fig. 1. (b): PL intensity at 3 eV as a function of the phosphorus content.

ergy, the lifetimes were obtained by a fitting procedure with a single exponential function of time-resolved PL data at several spectral positions, as shown in Fig. 6, where full lines represent the best fit curves. We found a slight dispersion of the lifetime inside the emission band: τ varies from 6.9 ms at E_{em}=2.7 eV to 5.1 ms at E_{em}=3.2 eV. Such dispersion of the lifetime corresponds to a progressive red shift of the emission peak of Fig. 5 during the decay, due to the low-energy tail of the signal decaying slower than the right tail.

We also studied the dependence on temperature of the luminescence signal measured by exciting at 4.8 eV in the central sample region. Figure 7 shows the PL spectra under laser excitation at 4.8 eV at different temperatures. Notwithstanding a certain degree of scattering of data points, from this investigation we can clearly see that the emission intensity excited at 4.8 eV is poorly dependent on temperature in the range 10–300 K. (inset of Fig. 7); also the peak position and width do not depend significantly on temperature. The lifetime τ measured on the peak, at 3 eV, is independent of temperature as well within experimental accuracy, as shown in Fig. 8(a), where several decay curves at various temperatures are reported. Performing the same investigation on the left tail of the band, a small variation in the τ value with the temperature appears [full circles and triangles in Fig. 8(b)]. This may suggest the existence of another small component centered at energies <2.8 eV. This secondary effect needs a specific investigation but it will not be analyzed in the present paper. It is worth noting, however, that the presence of this component may contribute to the observed asymmetry of the emission band.

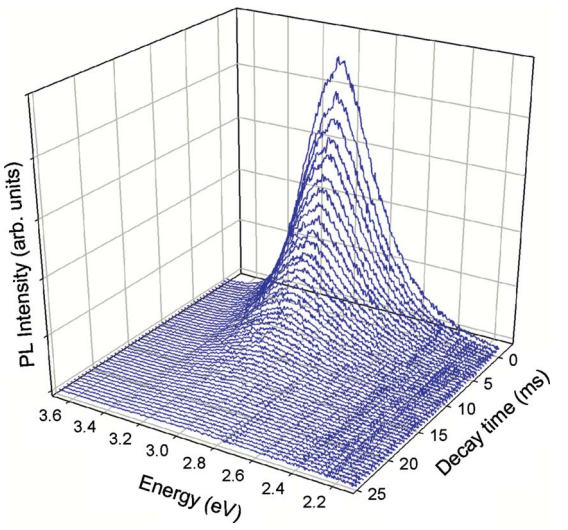

FIG. 5. (Color online) Time resolved PL spectra measured under laser excitation at 4.8 eV with W_T=500 μs and T_D from 1 μs to 25 ms.

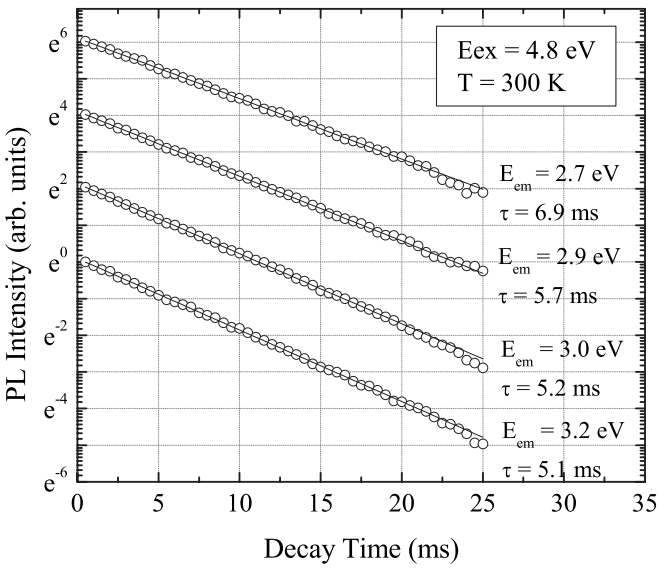

FIG. 6. Decay curves detected at room temperature at different emission energies (E_{em}) under laser excitation at E_{ex}=4.8 eV (W_T=500 μs and T_D from 1 μs to 25 ms). For viewing purposes, the initial values of the decay curves are arbitrarily scaled. Full lines represent the best fit curves by a single exponential equation.

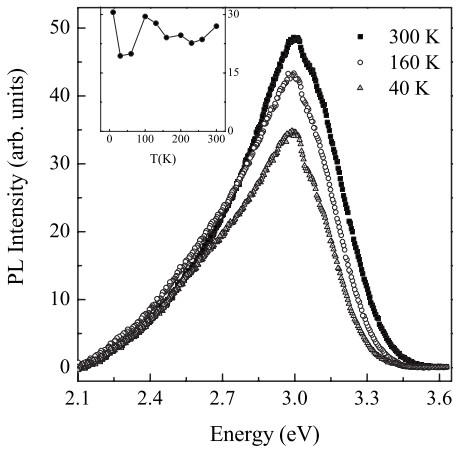

FIG. 7. PL bands under laser excitation at 4.8 eV in the central sample zone detected at various temperatures. The inset shows the temperature dependence of the integrated PL intensity.

Additionally, we performed ESR measurements both on pristine and x-ray irradiated preform samples aiming to explore the local arrangements of P atoms in the SiO_2 matrix, as well as the radiochemical processes activated by *X* irradiation. The pristine samples did not show any detectable paramagnetic defects. After a total deposited 10 keV *x*-dose of 20 kGy, at a dose rate=0.1 kGy/s, the ESR spectrum shows a structured signal extended over 10 mT, and shown in Fig. 9(a). The measurement was performed with a modulation amplitude of 0.1 mT and a nonsaturating microwave power of 0.19 mW. By comparison with literature, most of the observed signal can be ascribed to POHC-type defects.[8] Specifically, the negative peaks at 341.9 and 346.5 mT [marked as (1)] are associated to *r*-POHC, while the two additional peaks at 342.8 and 347.3 mT [marked as (2)] are characteristic features of l-POHC. While these well resolved peaks allow to clearly identify the two defects, the corresponding positive portions of the ESR signals overlap and cannot be singled out.[8] Specifically, by comparison with the published lineshapes of *r*-POHC and l-POHC,[8] it can be argued than the positive portions for $B < 341.5$ mT and for $345.5\ \text{mT} < B < 346.2$ mT are due to some linear combination of l-POHC and r-POHC. The coefficients of this combination, which could be determined in principle by computer

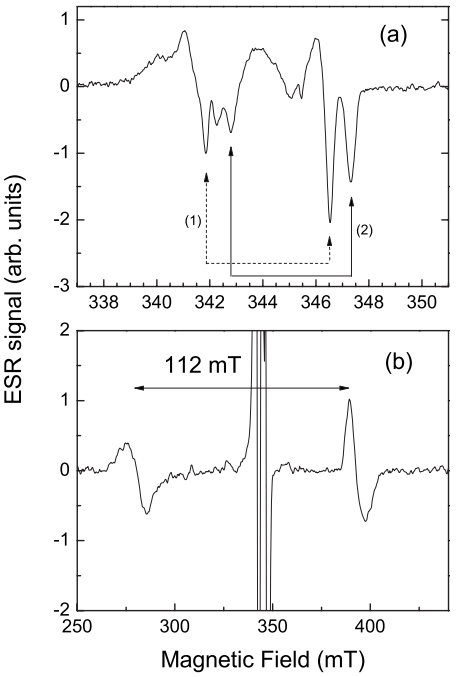

FIG. 9. Electron spin resonance spectrum detected in P-doped preform after a total deposited x-dose of 20 kGy. The signal in panel (a) was acquired by using a modulation amplitude of 0.1 mT and a 0.19 mW power. (1) and (2) indicate characteristic features of r-POHC and l-POHC, respectively. The spectrum in panel (b) was acquired by using a modulation amplitude of 0.5 mT and a 1.9 mW power. We verified both values of power to be below the saturation threshold of the respective signals.

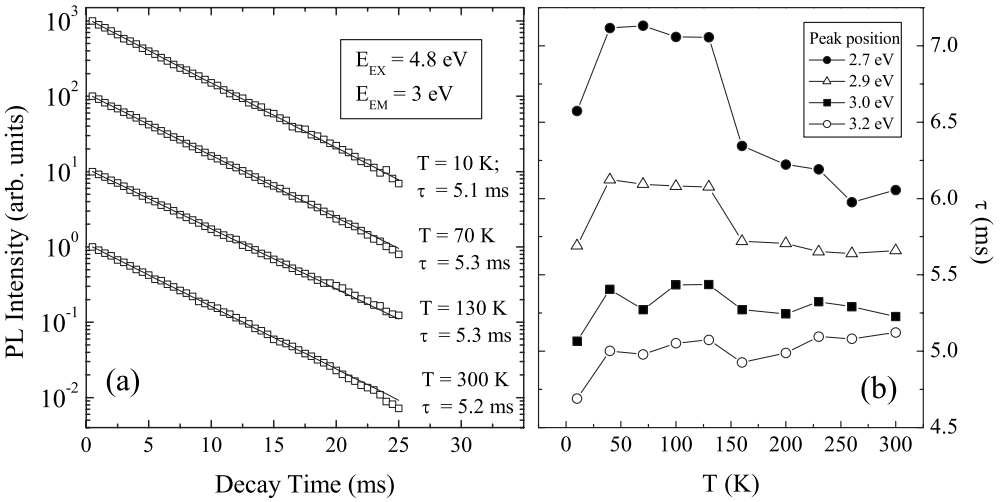

FIG. 8. (a): Decay curves detected at E_{em}=3 eV at different temperatures under laser excitation at E_{ex}=4.8 eV (W_T=500 μs and T_D from 1 μs to 25 ms). For viewing purposes, the initial values of the decay curves are arbitrarily scaled. Full lines represent the best fit curves by a single exponential equation. (b): Temperature lifetimes dependency at different energetic positions inside the 3 eV PL band at E_{ex} = 4.8 eV under laser excitation.

simulation of the measured lineshape, are of no concern for the present purposes. Both signals are actually hyperfine doublets with ~5 mT splitting, due to the interaction with the ^{31}P nucleus (100% natural abundance). It is worth noting that the observation of l-POHC contrasts with previous suggestions of this center being metastable at room temperature.[8] Finally, the central part of the spectrum also shows an additional structure around 344 mT of unknown origin. Since the contribution of the latter defect to the overall signal is minor, the overall concentration of POHCs can be estimated in good approximation by double integration of the whole spectrum in Fig. 9(a) and comparison with a reference sample. In this way we get: $(\mathrm{POHC})=(1.2\pm0.1)\times10^{17}$ cm^{-3}.[22] By scanning a wider magnetic-field range [Fig. 9(b)], we observe a hyperfine doublet with 112 mT separation which is consistent with the spectral features of the P2 defect, i.e., a four-fold coordinated P trapping an unpaired electron.[8] The substantially larger hyperfine splitting as compared to POHC is due to the much stronger localization of the unpaired electron on the P nucleus. This measurement was carried out with a modulation amplitude of 0.5 mT and a nonsaturating microwave power of 1.9 mW. The concentration of P2 centers can be estimated to be $(\mathrm{P2})=(1.4\pm0.1)\times10^{17}$ cm^{-3} and thus is consistent with (POHC) within experimental error. Finally, by PL measurements in this sample we observed a 42% reduction of the intensity of the native PL band at 3.0 eV.[23] The same measurements were performed on another sample irradiated with a lower (2 kGy) dose, where we found similar results: the emission intensity was reduced of 30%, while from ESR measurements we get: $(\mathrm{POHC})=(\mathrm{P2})=(8.5\pm0.8)\times10^{16}$ cm^{-3}. In neither sample we observed the characteristic hyperfine doublets of P1 or P4 centers.[8,10] This suggests that in these materials the twofold and three-fold coordinated configurations of P impurities are either present in much lower concentration or are much less sensitive to radiation than the tetrahedrical $[(\mathrm{O}\text{-})_3\mathrm{P}=\mathrm{O}]^0$ and $[(\mathrm{O}\text{-})_2\mathrm{P}(\text{-}\mathrm{O})_2]^+$ configurations acting as precursors for POHC and P2.

IV. DISCUSSION

Data in Figs. 3–8 demonstrate the existence in as-grown P-doped silica of an emission signal peaked at 3.0 eV and featuring two excitation channels at 4.8 and 6.4 eV. The lowest-energy excitation is detectable as well as a weak absorption band. The spatial dependence of the signal intensity in Fig. 4 strongly suggests this emission to be associated to a P-related defect. The fact that the spatial extension of the luminescent region is narrower than that of the P-doped zone, implies that the concentration of the specific center responsible for this emission is not strictly linearly correlated with the overall P concentration [see Fig. 4(b)]. Specifically, data in Fig. 4 suggest the emitting center to be formed in detectable concentrations only when the overall P content overcomes a threshold of about 4%.

The main spectroscopic features of this PL signal are its long lifetime in the ms range and its weak dependence on temperature. The first result suggests the emission to originate from a spin-forbidden transition from an excited triplet state (T_1). At the same time, the temperature independence implies the absence of efficient nonradiative decay channels from T_1 to the ground state, so that the ~6 ms lifetime has to be interpreted as a purely radiative decay lifetime. Finally, the dispersion of the radiative decay lifetime within the emission band suggests strong inhomogeneity effects to affect the overall width of the band, as recently pointed out for other defects embedded in an amorphous matrix.[18] Data analysis aimed to quantitatively estimate the degree of inhomogeneity of the band is in progress, being complicated by the possible presence of another weaker signal on the left side of the band.

The first-excitation peak at 4.8 eV detected by the PLE measurement is likely to be related to the 4.8 eV band found in the OA spectrum of the defect (Fig. 2). However, it can be argued that the 3.0 eV luminescent band cannot be the inverse transition of the 4.8 eV absorption.

To demonstrate this assertion, we evaluate the oscillator strength f of the 4.8 eV peak as if the 3.0 eV was its inverse transition. Using *Smakula's equation*[19] we evaluate the product Nf, where N is the defects concentration:

$$Nf = n\left(\frac{E_0}{E_{eff}}\right)^2 \alpha_{\max}\Gamma\Delta\left(\frac{m_e c}{2\pi^2 e^2 \hbar}\right) \approx n\left(\frac{E_0}{E_{eff}}\right)^2 \alpha_{\max}\Gamma\Delta \times 9.111\times10^{15}[\mathrm{eV}^{-1}\ \mathrm{cm}^{-2}], \quad (1)$$

n is the refractive index of our samples, $(E_{eff}/E_0)^2$ is the effective field correction,[19] $\alpha_{\max}$ is the amplitude and Δ is the full with at half maximum (FWHM) of OA band, Γ is a numeric coefficient which depends on the bandshape and $m_e, c, \hbar$ have their usual meaning.

If we consider that $\Gamma\approx1.0645$ for a Gaussian shape, and $n(E_0/E_{eff})^2$ for silica is close to unity throughout the IR to near-UV spectral range, Eq. (1) becomes:

$$Nf \approx \alpha_{\max}\Delta \times 9.699\times10^{15}[\mathrm{eV}^{-1}\ \mathrm{cm}^{-2}]. \quad (2)$$

To evaluate the product $\alpha_{\max}\Delta$, we performed a Gaussian fit of the OA peak at ~4.8 eV of the inset of Fig. 2, imposing the same FWHM of the 4.8 eV PLE band (0.7 eV) [Fig. 3(b)], and finding $\alpha_{\max}=0.10$ cm^{-1}. From this calculation we obtain:

$$\alpha_{\max}\Delta \simeq 0.07\ \mathrm{eV\ cm}^{-1}, \quad (3)$$

$$Nf = 6.79\times10^{14}\ \mathrm{cm}^{-3}. \quad (4)$$

The oscillator strength is related to the radiative decay time τ of the inverse emission by:[19]

$$f \approx \frac{1}{(\hbar\omega)^2\tau}\left(\frac{E_0}{E_{eff}}\right)^2\frac{1}{n}\times2.305\times10^{-8} \approx \frac{1}{(\hbar\omega)^2\tau}\times\frac{1}{n^2}\times2.305\times10^{-8} = 1.18\times10^{-7}, \quad (5)$$

where $n=1.466$ and $\hbar\omega$ represents the *zero phonon line* energy position, roughly half way between absorption and emission: $\hbar\omega = 3.7$ eV.

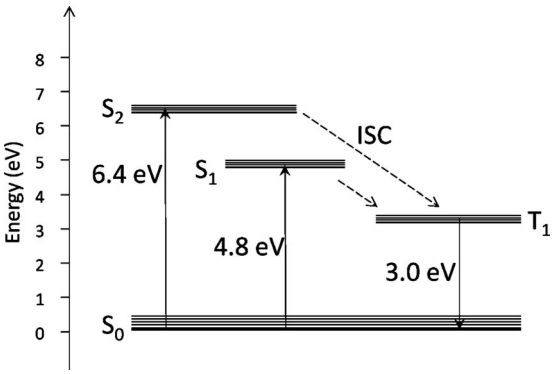

FIG. 10. Electronic levels scheme of the diamagnetic P-related defect supposed to be at the origin of the observed optical activity. Solid arrows indicate the radiative transitions in absorption and luminescence. Dashed arrows indicate the ISC nonradiative transitions from S_1 or S_2 to T_1.

From Eqs. (4) and (5), with $\tau = 6$ ms, we finally obtain:

$$N \simeq 6 \times 10^{21} \text{ cm}^{-3}. \quad (6)$$

This concentration value is higher than the maximum phosphorus concentration in our samples (7.09 wt. % in zone 4 corresponds to $[P]=3.0\times10^{21}$ cm^{-3}). Also, ESR data discussed below show that the concentration of the luminescent defect is in the order of 10^{17} cm^{-3}. Hence, we consider really improbable for the 3.0 eV PL band to be the inverse transition of the 4.8 eV OA. On the contrary, assuming a nondegenerate singlet ground state S_0 for the defect, the 4.8 eV band must arise from an allowed $S_0 \rightarrow S_1$ transition. Also, the second PLE peak at 6.4 eV, whose intensity is comparable to the 4.8 eV component, must be associated to a $S_0 \rightarrow S_2$ transition to an upper excited state. Given the absence of any other emission signals upon 4.8 or 6.4 eV excitations, the decay from these two excited levels (S_1, S_2) to the emitting 3.0 eV state (T_1) must occur by a very efficient intersystem crossing (ISC) process active at all temperatures. Based on these considerations, we can propose for the P-related luminescent defect the level scheme in Fig. 10.

Contrastingly, the 6.9 eV absorption band is due to another diamagnetic P-related defect, unrelated to the emitting center. As a matter of fact, the 6.4 eV peak in the PLE signal occurs in a spectral region where the absorption is almost zero [compare Fig. 2 and 3], while the excitation of the sample at 6.9 eV did not result in any measurable emission at any temperature. The 6.4 eV OA band which, based on PLE data, one may expect to find in the OA spectrum with comparable intensity to the 4.8 eV, is likely to be buried under the intense 6.9 eV peak.

Indications on the microscopic structure of the luminescent P-related defect can be drawn from the explorative ESR measurements described in the previous section. Several evidences in literature lead to the assumption that in phosphosilicate glass most of P atoms are arranged as $[(O\text{-})_3P{=}O]^0$ tetrahedra.[13–16] The other possible defective arrangements of P in silica have been proposed based on ESR data, and are expected to be present only in minor concentrations. ESR data on each of the two irradiated preforms reveal POHC and P2 defects induced by x-rays in about the same concentration. This finding is consistent with a scheme in which the formation of the two paramagnetic defects is correlated, and occurs by trapping on Si-substitutional P centers $[(O\text{-})_2P(\text{-}O)_2]^+$ of the electron made available by ionization of $[(O\text{-})_3P{=}O]^0$.[24] Similar correlated POHC-P2 formation under laser irradiation has been observed in a recent study on P-doped SiO_2 glass.[6] In this context, the concurrent observation of a partial bleaching of the 3.0 eV emission band upon irradiation, leads to tentatively identify the luminescent center with one of the two precursors, i.e., the most likely microscopic structure of the emitting diamagnetic defect is either $[(O\text{-})_3P{=}O]^0$ or $[(O\text{-})_2P(\text{-}O)_2]^+$. A 42% reduction in the PL accompanied by the formation of $(1.2\pm0.1)\times10^{17}$ cm^{-3} paramagnetic defects implies a concentration of $(2.8\pm0.3)\times10^{17}$ cm^{-3} for the luminescent center in the unirradiated sample.[25] Comparing with $[P]=3.0\times10^{21}$ cm^{-3} in zone 4, we see that the $[(O\text{-})_3P{=}O]^0$ model is unlikely, since literature data strongly suggest that this structure should be present in concentrations much higher than 10^{17} cm^{-3}, and possibly close to the total P content. This conclusion is consistent also with the lack of a strict linear correlation between the overall concentration of P and that of the luminescent defect [Fig. 4(b)]. Hence, present data suggest the diamagnetic Si-substitutional P impurity, $[(O\text{-})_2P(\text{-}O)_2]^+$, as a tentative microscopic model of the luminescent center. Our model of the emitting defect and of the conversion process activated by *X* radiation is represented in Fig. 11. By comparing the concentration inferred above with the intensity of the 4.8 eV band, one can estimate the oscillator strength $f \sim 2\times10^{-3}$ of the $S_0 -> S_1$ transition. Computational studies may help now to find out if these optical properties are consistent with those expected for a Si-substitutional P impurity.

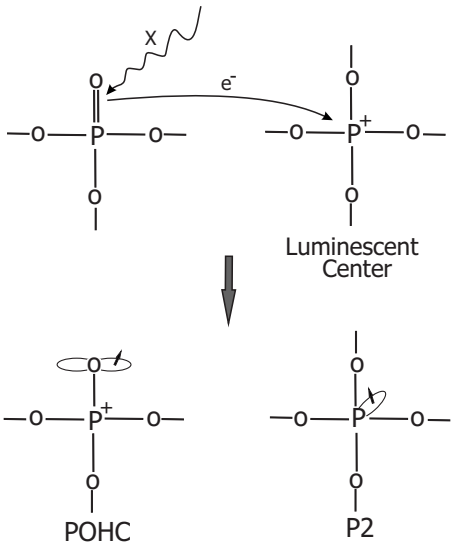

FIG. 11. Graphical representation of the photochemical processes activated by x-rays in the P-doped preform sample, and of the model proposed (upper right structure) for the luminescent defect responsible for the 3.0 eV emission band.

V. CONCLUSIONS

By luminescence measurements on step-index P-doped SiO_2 fiber preforms, carried out under excitation by laser and synchrotron UV and VUV light, we detect an optical activity consisting in a long-lived (~6 ms radiative lifetime) and temperature-independent luminescence emission peaked at 3.0 eV, featuring two excitation bands centered at 4.8 and 6.4 eV. The 4.8 eV transition can be also revealed as a weak band in the optical absorption spectrum of the preform. The spatial profile of the PL intensity on the preform is consistent with that of P doping, thus allowing the attribution of this optical activity to a P-related point defect. The detailed study of the spectroscopic features of the defect allows to propose a scheme of its electronic transitions, comprising two singlet (S_1,S_2) and one triplet (T_1) excited levels, where the long-lived emission is due to the spin-forbidden transition to the ground state from the excited triplet populated by very efficient nonradiative decay from S_1 and S_2. PL and ESR measurements on *X*-irradiated samples allow to propose a microscopic model for the defect consisting in a four-coordinated diamagnetic P impurity substitutional to Si atoms in the SiO_2 matrix.

ACKNOWLEDGMENTS

We acknowledge financial support received from the project "P. O. R. Regione Sicilia-Misura 3.15-Sottoazione C." The authors would like to thank G. Napoli and G. Lapis for assistance in cryogenic work. Finally, we are grateful to all the members of the LAMP research group (http://www.fisica.unipa.it/amorphous/) for support and enlightening discussions.

*fmessina@fisica.unipa.it

[1] G. Keiser, *Optical Fiber Communications*, 2nd ed. (McGraw-Hill, New York, 1991).
[2] D. Ehrt, P. Ebeling, and U. Natura, J. Non-Cryst. Solids **263-264**, 240 (2000).
[3] P. C. Becker, N. A. Olsson, and J. R. Simpson, *Erbium-Doped Fiber Amplifiers: Fundamentals and Technology* (Academic Press, London, 1999).
[4] M. C. Paul, D. Bohra, A. Dhar, R. Sen, P. K. Bhatnagar, and K. Dasgupta, J. Non-Cryst. Solids **355**, 1496 (2009).
[5] B. Malo, J. Albert, F. Bilodeau, T. Kitagawa, D. C. Johnson, K. O. Hill, K. Hattori, Y. Hibino, and S. Gujrathi, Appl. Phys. Lett. **65**, 394 (1994).
[6] H. Hosono, K. Kajihara, M. Hirano, and M. Oto, J. Appl. Phys. **91**, 4121 (2002).
[7] R. A. Weeks and P. J. Bray, J. Chem. Phys. **48**, 5 (1968).
[8] D. L. Griscom, E. J. Friebele, and K. J. Long, J. Appl. Phys. **54**, 3743 (1983).
[9] W. L. Warren, M. R. Shaneyfelt, D. M. Fleetwood, and P. S. Winokur, Appl. Phys. Lett. **67**, 995 (1995).
[10] P. Ebeling, D. Ehrt, and M. Friedrich, Opt. Mater. **20**, 101 (2002).
[11] G. Pacchioni, D. Erbetta, D. Ricci, and M. Fanciulli, J. Phys. Chem. B **105**, 6097 (2001).
[12] J. W. Chan, T. Huser, J. S. Hayden, S. H. Risbud, and D. M. Krol, J. Am. Ceram. Soc. **85**, 1037 (2002).
[13] U. Hoppe, G. Walter, A. Bartz, D. Stachel, and A. Hannon, J. Phys.: Condens. Matter **10**, 261 (1998).
[14] R. K. Brow, J. Non-Cryst. Solids **263-264**, 1 (2000).
[15] V. G. Plotnichenko, V. O. Sokolov, V. V. Koltashev, and E. M. Dianov, J. Non-Cryst. Solids **306**, 209 (2002).
[16] C. R. G. Walter and G. Goerigk, J. Non-Cryst. Solids **352**, 4051 (2006).
[17] S.-I. Kitazawa, S. Yamamoto, M. Asano, and S. Ishiyama, Physica B **349**, 159 (2004).
[18] M. D'Amico, F. Messina, M. Cannas, M. Leone, and R. Boscaino, Phys. Rev. B **78**, 014203 (2008).
[19] G. Pacchioni, L. Skuja, and D. L. Griscom, *Defects in* SiO_2 *and Related Dielectrics: Science and Technology* (Kluwer, Dordrecht, 2000).
[20] In P4, the P atom hosts an additional lone pair, not represented.
[21] In the two-fold coordinated precursor of P4 center, the P atom hosts an additional lone pair, not represented.
[22] This estimate is based on the assumption that P-related paramagnetic centers are uniformly distributed in all the P-doped volume. If one assumes instead, following the results of Fig. 4(b), that the paramagnetic centers are located in zones III and IV only (as the luminescence signal is), a correction factor must be applied, leading to a higher estimate: $(3.2 \pm 0.3) \times 10^{17}$ cm^{-3}. Under this hypothesis, all the other concentration values reported later on must be scaled for the same factor.
[23] The bleaching of the PL signal is accompanied by the appearance of absorption signals which will be not discussed here. However it is worth noting that the induced absorption at 4.8 eV (~0.1 optical density) is not sufficiently intense to compromise the measurement of luminescence intensity.
[24] The observation of both l-POHC and r-POHC, according to Griscom's model, may slightly modify this interpretation by suggesting that a significant fraction of ionized P sites feature two doubly-bonded nonbridging O atoms instead of one.
[25] This line of reasoning still holds if one uses the higher estimate of the concentration of paramagnetic defects obtained by assuming them to be present only in zones III and IV.